Altered Topological Structure of the Brain White Matter in Maltreated Children through Topological Data Analysis

Tahmineh Azizi[1], Moo K. Chung[1,*], Jamie Hanson[2], Thomas Burns[3], Andrew Alexander[4], Richard Davidson[5], Seth Pollak[5]

1 Department of Biostatistics and Medical Informatics, University of Wisconsin-Madison, USA
2 Department of Psychology, University of Pittsburgh, USA
3 Okinawa Institute of Science and Technology (OIST) Graduate University, Japan
4 Department of Medical Physics, University of Wisconsin-Madison, USA
5 Department of Psychology, University of Wisconsin-Madison, USA

*Correspondence: Moo K. Chung, Email: `mkhung@wisc.edu`.

Abstract

Childhood maltreatment may adversely affect brain development and consequently behavioral, emotional, and psychological patterns during adulthood. In this study, we propose an analytical pipeline for modeling the altered topological structure of brain white matter structure in maltreated and typically developing children. We perform topological data analysis (TDA) to assess the alteration in global topology of the brain white-matter structural covariance network for child participants. We use persistent homology, an algebraic technique in TDA, to analyze topological features in the brain covariance networks constructed from structural magnetic resonance imaging (MRI) and diffusion tensor imaging (DTI). We develop a novel framework for statistical inference based on the Wasserstein distance to assess the significance of the observed topological differences. Using these methods in comparing maltreated children to a typically developing sample, we find that maltreatment may increase homogeneity in white matter structures and thus induce higher correlations in the structural covariance; this is reflected in the topological profile. Our findings strongly demonstrates that TDA can be used as a baseline framework to model altered topological structures of the brain.

1 Introduction

Child maltreatment can have severe life-long mental, emotional, physical, and sexual health outcomes [102]. These serious long-term consequences are notable given that the U.S. Department of Health and Human Services estimates over 680,000 children suffer different forms of maltreatment, such as child abuse or neglect every year. Many of the adverse impacts likely emerge through changes in neurobiology such as reducing brain volumes or brain connectivity [45]. Indeed, a growing body of scientific research finds altered brain functioning in those who have suffered early childhood abuse and neglect [41, 69, 85, 103]. For example, multiple studies have found maltreatment in childhood may cause a decrease in volume of the corpus callosum, the largest white matter structure in the brain critical for interhemispheric communication [69, 103]. Similarly, neglected children have smaller pre-frontal cortex volumes, which helps in

behavior, emotion, and cognition regulation [70, 98]. These neurological changes, especially in brain connectivity may have a deep influence on children's emotional, social and behavioral functioning [47, 98].

Both structural- and diffusion-MRI can facilitate studies on the impact of abuse and neglect on brain development during childhood [40, 48, 66, 74]. To quantify the variation in neuroanatomical shapes using tensor-based morphometry (TBM), the spatial derivatives of deformation fields can be obtained via nonlinear image registration applied in warping individual structural-MRI to a template [19, 95]. The Jacobian determinant from the warping measures the volumetric changes in brain tissue at the voxel level [19, 24, 29, 67, 96]. At each voxel, a linear model is set up to take the tensor maps such as the Jacobian determinant as a response variable in order to obtain voxel-level statistics. Univariate-TBM has been widely used in the field. However, when we perform hypothesis testing on multiple anatomical brain regions, the univariate framework may fail to relate how the volume change in one voxel relates to other voxels. Thus, there is a need to model the Jocobian determinant in a network analysis fashion and relate variations in one region to another region through structural covariance [8, 42, 43, 61, 78, 104, 105].

Graph theory based methods have been frequently used to uncover the topological properties of brain networks including the investigation of topological alterations in white matter for neuromyelitis optica [64], exploring abnormal topological organization in the structure of cortical networks in Alzheimer's disease (AD) [65], alterations in the topological properties of the anatomical network in early blindness [86], abnormal topological changes during AD progression [22, 56, 76]. Graph theory also has been used to measure and evaluate the integration and segregation of the brain network [56, 80]. In the standard graph theory based brain network analysis, graph features such as node degrees and clustering coefficients are obtained after thresholding connectivity matrices [12, 13, 99]. Depending on the choice of these thresholds, the final statistical results can be drastically different [14, 15, 59]. Thus, there is a practical need to develop a *multiscale* network analysis framework that provides a consistent result and interpretation regardless of the choice of thresholding. Persistent homology offers one possible solution to the multiscale problem. Instead of studying networks at a fixed scale, persistent homology summarizes the changes of topological features over different scales and finds the most persistent topological features that are robust to perturbations. This robust performance under different scales is needed for network models that are parameter and scale dependent. In persistent homology, instead of building networks at one fixed parameter that may not be optimal, we analyze the collection of networks over every possible thresholds [58, 59]. It has been shown that the persistent homology approach can be effectively used to overcome the problem related to the arbitrariness of thresholding [57]. Persistent homology can detect subtle topological differences between networks while existing statistical models might fail to differentiate the differences [75, 89, 110]. In [63], persistent homology has been applied to characterize the neuropsychological properties of the brain. In [107], persistent homology has been used to study the evolution of a spatiotemporal brain network of Alzheimer's disease (AD). They have also proposed that persistent homology can be considered as a framework to assess the neurophysiological properties of image quality. Topological data analysis has been applied to brain networks to classify altered brain states [9]. Topological data analysis also has been used to extract the topology of brain connectomes in attention deficit hyperactivity disorder (ADHD) [37]. One important application for TDA is facilitating EEG signal analysis using the geometrical and topological tools such as persistent homology [53, 73, 100].

To analyze the structural covariance, we propose to use persistent homology, a main tool in topological data analysis (TDA) [10, 14, 18, 32, 34, 58, 59, 87]. Topological data

analysis has been widely used as a popular method to analyze feature spaces with high dimensionality without the prerequisite to consider specific modeling assumptions [32]. Persistent homology as a recently developed branch in TDA defines a powerful mathematical framework for understanding, characterizing and quantifying topology of networks [18, 30, 34, 58, 59]. Persistent homology provides a general framework based on algebraic topology, and gives a novel solution to the multi-scale network analysis challenge [32, 101]. In persistent homology, rather than examining networks using graphs at one fixed scale at a time [30, 34], the persistent homology technique identifies persistent topological features that are robust across different scales. The persistence diagram (PD) demonstrates the persistence of topological features over various scales which plays the role of an indicator in displaying the birth and death times of the holes or cycles as we change the scale. The important topological invariants called the Betti number counts the number of holes in networks, and can be used to visualize and quantify underlying topology. Betti curves, which plots the Betti numbers over changing scales, have been used to detect the abnormal functional brain networks in the study of the alterations of AD progression [56]. There exists a wide range of quantitative persistent homology features, such as: persistence landscapes (PL) [6], persistent entropy (PE) [81], persistence images (PI) [1] which have been used to analyze and compare brain networks of different patients [9].

In this study, we propose to use TDA tools to assess the topological changes of white matter structures. The present study aims to explore the variation in topological features in the structural covariance of brain's children white matter who experience maltreatment by applying several techniques in persistent homology. Particularly, we are interested in characterizing abnormal changes and alteration in maltreated children brain's white matter using the Jacobian determinant in the tensor-based morphometry (TBM) from structural-MRI and fractional anisotropy (FA) values from diffusion-MRI. Since the changes in one voxel is related to other voxels, and the univariate-TBM might be unable to characterize these subtle variations across different voxels while the persistent homology can test more complex network hypotheses across brain regions. We characterize the topological properties of the networks using the Betti curves. We apply the Wasserstein distance (WS) between the birth and death values associated with the Betti curves. Then, we develop a statistical inference procedure in measuring topological differences between the groups. TDA effectively provides a comprehensive framework to characterize the persistence of topological structures such as connected components and cycles at different scales in brain networks of maltreated and typically developing children. Our results demonstrate significant altered topological structure of white matter for maltreated children relative to normal controls. In particular, we observe higher number of connected components in typically developing children. This indicates more heterogenous white matter structures compared to maltreated children.

2 Methods

Since child maltreatment may affect brain development during adolescent, to track the trajectories of brain development after damages caused by abuse and neglect, we need to model the changes happen in local and global structure of brain networks at different scale. To understand the topological alteration of the structural brain network, we use mathematical and computational techniques in topological data analysis (TDA) (Figure 1). Within TDA, we can comprehend the variations in topological structure of brain networks.
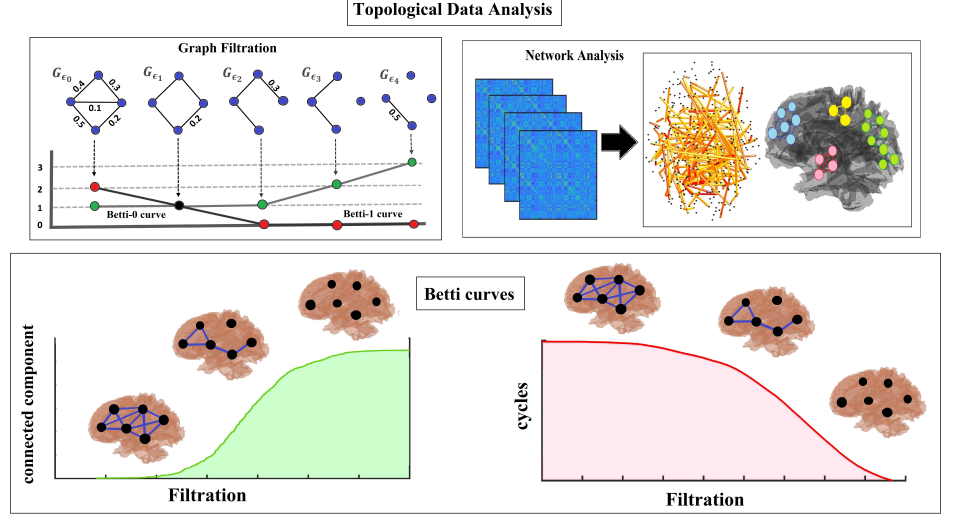
Figure 1. Proposed TDA pipeline for studying structural covariance networks. Studying the network topology has given rise to developing new frameworks to study the scale and dimensionality of brain networks. The topological data analysis aims to extract the topological features of brain network using the tools at the interface of geometry and topology.

2.1 Birth and death decomposition

We model brain networks as weighted graphs. Suppose we have the weighted graph $G(V, w)$ where $V = \{1, 2, \ldots, q\}$ defines the node set and $w = (w_{ij})$ defines edge weights. There are total $k = (q^2 - q)/2$ number of edges. We can treat the weighted graphs as simplicial complexes [31, 111]. A most well known simplicial complex is the Rips complex $\mathcal{R}_\epsilon$ which is defined as a simplicial complex consisting of k-simplices composed of $k + 1$ nodes within distance ϵ [34]. For q number of nodes, a graph includes at most 1-simplices while a Rips complex contains at most $(q - 1)$-simplices. For a network with q nodes, the graph will include simplices of dimension zero and one. The following hierarchical nesting structure called the *Rips filtration* is induced by the Rips complex:

$$R_{\epsilon_0} \subset R_{\epsilon_1} \subset R_{\epsilon_2} \subset \ldots \tag{1}$$

where $0 = \epsilon_0 < \epsilon_1 < \epsilon_2 < \ldots$ are called the filtration values. When the number of nodes becomes large, the Rips complex becomes very dense and often causes serious computational bottlenecks in tasks such as the permutation test. For this reason, we propose to use the graph filtration, a special case of reduced Rips filtration [58, 59]. Define the binary graph $G_\epsilon = (V, w_\epsilon)$ with binary edge weights $w_\epsilon = (w_{\epsilon, ij})$ such that

$$w_{\epsilon, ij} = \begin{cases} 1 & \text{for } w_{ij} > \epsilon, \\ 0 & \text{otherwise.} \end{cases} \tag{2}$$

The binary matrix w_ϵ might be interpreted as the adjacency matrix of G_ϵ and defines a simplicial complex including 0-simplices (nodes) and 1-simplices (edges) only [59]. We then obtain the graph filtration of G as a sequence of nested multi-scale binary graphs of form:

$$G_{\epsilon_0} \supset G_{\epsilon_1} \supset \cdots \supset G_{\epsilon_k} \tag{3}$$

with filtration values $\epsilon_0 < \epsilon_1 < \epsilon_2 < \cdots < \epsilon_k$ [58]. We have represented the schematic of graph filtration of a graph G with four nodes in Figure 2.
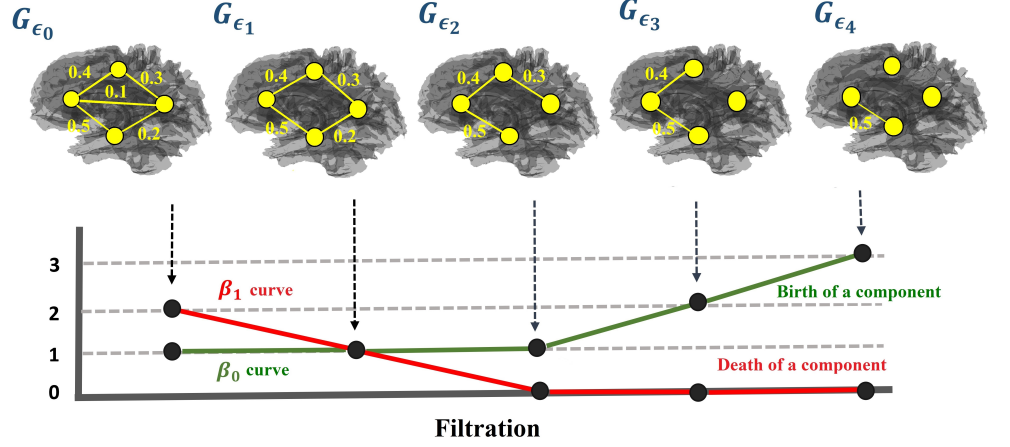
Figure 2. Example of a graph filtration on graph G, which induces a sequence of nested multiscale binary graphs of the form $G_{\epsilon_0} \supset G_{\epsilon_1} \supset G_{\epsilon_2} \supset G_{\epsilon_3} \supset G_{\epsilon_4}$ with filtration values $\epsilon_0 < \epsilon_1 < \epsilon_2 < \epsilon_3 < \epsilon_4$. During the filtration, connected components are born one after the other. Whereas, loops die one after the other. Thus, the β_0-curve is monotonically non-decreasing while the β_1-curve is monotonically non-increasing.

Variation of the filtration value ϵ may cause appearance or disappearance of connected components or loops [17]. In a simplical complex, the number of connected components is the Betti-0 number β_0 and the number of independent cycles (or loops) is the Betti-1 number β_1. In graph filtrations, β_0 increases while β_1 decreases over filtrations (Figure 2) [17]. During the graph filtration, a connected component that are born never dies, thus, the death time is infinity. Consequently, we ignore the death values of connected components and characterize by a set of increasing birth values $\mathcal{B}_G$:

$$\mathcal{B}_G : \epsilon_{b_1} < \cdots < \epsilon_{b_{m_0}}. \tag{4}$$

On the other hand, loops are always there in a complete graphs and thus the birth values of cycles are considered as $-\infty$ and ignored. Then the loops are completely characterized by the a set of increasing death values $\mathcal{D}_G$:

$$\mathcal{D}_G : \epsilon_{d_1} < \cdots < \epsilon_{d_{m_1}}. \tag{5}$$

Then we can decompose edge weights uniquely into the birth set $\mathcal{B}_G$ and death set $\mathcal{D}_G$ through the *birth-death decomposition* [91]:

Theorem 2.1. *The edge weight set $w = (w_{ij})$ of a complete graph can be uniquely decomposed as*

$$w = \mathcal{B}_G \cup \mathcal{D}_G, \quad \mathcal{B}_G \cap \mathcal{D}_G \neq \emptyset, \tag{6}$$

where $\mathcal{B}_G = \{\epsilon_{b_1}, \epsilon_{b_2}, \ldots, \epsilon_{b_{m_0}}\}$ and $\mathcal{D}_G = \{\epsilon_{d_1}, \epsilon_{d_2}, \ldots, \epsilon_{d_{m_1}}\}$ with $m_0 = q - 1$ and $m_1 = (q-1)(q-2)/2$. The $\mathcal{B}_G$ forms the persistent diagram for 0D homology (connected components) and $\mathcal{D}_G$ forms the persistent diagram for 1D homology (cycles).

We can show that the birth set $\mathcal{B}_G$ forms the maximum spanning tree (MST) of G while the death set $\mathcal{D}_G$ are edges that do not belong to MST. Subsequently, we compute the Betti-0 curves by using the Kruskal's algorithm which works by identifying the minimum spanning tree to construct Betti-0 curves [59]. Then Betti-1 curves are identified through the Euler characteristic [16, 17]. The computation can be done in $\mathcal{O}(q \log q)$ runtime.
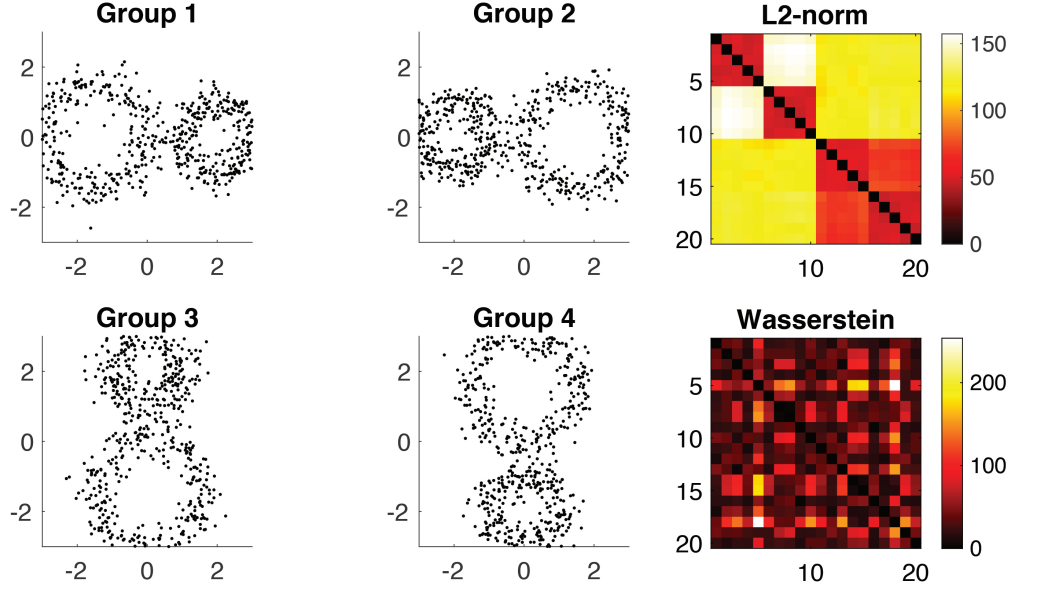
Figure 3. Topological distance between topologically equivalent networks. Group 1 Groups 2 and 3 and 4 are generated by rotating Group 1 networks

2.2 Wasserstein distances between networks

The topological distance between persistent diagrams are often measured using the 2-Wasserstein distance. For graph filtrations, the Wasserstein distance between persistent diagrams can be computed through the order statistics on edge weights [90]. Suppose we have two networks $G_1 = (V^{G_1}, w^{G_1})$ and $G_2 = (V^{G_2}, w^{G_2})$ with q number of nodes. Assume the birth and death sets are

$$\mathcal{B}_{G_i} : \epsilon^i_{b_1} < \cdots < \epsilon^i_{b_{m_0}}, \tag{7}$$

$$\mathcal{D}_{G_i} : \epsilon^i_{d_1} < \cdots < \epsilon^i_{d_{m_1}}. \tag{8}$$

Then the 2-Wasserstein distance for connected components is given by

$$D^{0D}_W(G_1, G_2) = \sum_{i=1}^{m_0} [\epsilon^1_{b_i} - \epsilon^2_{b_i}]^2. \tag{9}$$

Similarly, the 2-Wasserstein distance for loops is given by

$$D^{1D}_W(G_1, G_2) = \sum_{i=1}^{m_1} [\epsilon^1_{d_i} - \epsilon^2_{d_i}]^2. \tag{10}$$

The 2-Wasserstein distance D^{0D}_W measures the topological difference related to the connected components while D^{1D}_W measures the topological difference related to loops. By combining D^{0D}_W and D^{1D}_W, we have the overall topological difference

$$D^{0,1}_W(G_1, G_2) = D^{0D}_W(G_1, G_2) + D^{1D}_W(G_1, G_2). \tag{11}$$

In application, we used three distances $D^{0D}_W, D^{1D}_W, D^{0,1}_W$. We will simply denote the distances in the application as $\mathcal{L}_{top}$ if there is no ambiguity.

To see the effect of the Wasserstein distance, we generated 4 circular patterns of identical topology (Figure 3). Along the circles, we uniformly sampled 60 nodes and

added Gaussian noise $N(0, 0.3^2)$ on the coordinates. We generated 5 random networks per group. The Euclidean distance (L_2-norm) between randomly generated points are used to build connectivity matrices. Figures 3 shows the superposition of nodes from 20 networks. Sine they are topologically equivalent, the distance between networks should show no clustering pattern. In fact the Wasserstein distance $D_W^{0,1}$ shows no discernible clustering pattern while L_2-norm shows the clustering pattern. The L_2-norm distance is particularly large between horizontal (Groups 1 and 2) and vertical patterns (Groups 3 and 4).

Assume we have two groups of networks $X = (X_1, \ldots, X_m)$ and $Y = (Y_1, \ldots, Y_n)$. If there is group difference, the topological distances are expected to be relatively small within groups and relatively large between groups. The average topological distance within the groups given by

$$\overline{\mathcal{L}}_W(X, Y) = \frac{\sum_{i<j} \mathcal{L}_{top}(X_i, X_j) + \sum_{i<j} \mathcal{L}_{top}(Y_i, Y_j)}{\binom{m}{2} + \binom{n}{2}}.$$

Similarly the topological distance between the groups is given by

$$\overline{\mathcal{L}}_B(X, Y) = \frac{\sum_{i=1}^{m} \sum_{j=1}^{n} \mathcal{L}_{top}(X_i, Y_j)}{mn}.$$

We then use the ratio statistic

$$\Phi_{\mathcal{L}}(X, Y) = \overline{\mathcal{L}}_B(X, Y) \Big/ \overline{\mathcal{L}}_W(X, Y)$$

for testing the topological difference between the groups of networks. If $\Phi_{\mathcal{L}}$ is large, the groups differ significantly in network topology. If $\Phi_{\mathcal{L}}$ is small, the group difference is small. Since the distributions of the ratio statistic $\Phi_{\mathcal{L}}$ is unknown, the permutation test is used to determine the empirical distributions. Since the permutation test is usually slow, we adapted a scalable online computation strategy called the *transposition test* as follows [20].

We first concatenate two groups X and Y and compute the distance matrix of size $(m + n) \times (m + n)$ for every pair of networks. After computing the distance matrix, we perform the permutation test by rearranging rows and columns based on the permuted group labels. Since we do not have to recompute the distances in each permutation, it drastically speed up the computation. To speed up the permutation further, we adapted the transposition test, the online version of permutation test [90]. The transposition between k-th and l-th networks between the groups is defined as

$$\pi_{kl}(X) = (X_1, \ldots, X_{k-1}, Y_l, X_{k+1}, \ldots, X_m), \tag{12}$$
$$\pi_{kl}(Y) = (Y_1, \ldots, Y_{l-1}, X_k, Y_{l+1}, \ldots, Y_n), \tag{13}$$

In transposition procedure, the ratio statistic changes from $\Phi_{\mathcal{L}}(X, Y)$ to $\Phi_{\mathcal{L}}(\pi_{kl}(X), \pi_{kl}(Y))$ over transposition π_{kl} and involves the following function:

$$v(X, Y) = \sum_{i<j} \mathcal{L}_{top}(X_i, X_j) + \sum_{i<j} \mathcal{L}_{top}(Y_i, Y_j), \tag{14}$$

$$w(X, Y) = \sum_{i=1}^{m} \sum_{j=1}^{n} \mathcal{L}_{top}(X_i, Y_j), \tag{15}$$

where v defines the total sum of within group distances and w presents the total sum of between group distances. When X_k and Y_l are swapped, the function v changes over the transposition π_{kl} as the form:

$$v(\pi_{kl}(X), \pi_{kl}(Y)) = v(X, Y) + \delta(X, Y), \tag{16}$$

where

$$\delta(X, Y) = \sum_{i \neq k} \mathcal{L}_{top}(Y_l, X_i) - \sum_{i \neq k} \mathcal{L}_{top}(X_k, X_i) + \sum_{i \neq l} \mathcal{L}_{top}(X_k, Y_i) - \sum_{i \neq l} \mathcal{L}_{top}(Y_l, Y_i). \quad (17)$$

Similarly, we can find how function w changes iteratively over the transposition π_{kl} as the form:

$$w(\pi_{kl}(X), \pi_{kl}(Y)) = w(X, Y) - \delta(X, Y) \quad (18)$$

Finally, the ratio statistics over the transposition is computed as

$$\Phi_{\mathcal{L}}(\pi_{kl}(X), \pi_{kl}(Y)) = \frac{w(\pi_{kl}(X), \pi_{kl}(Y))}{v(\pi_{kl}(X), \pi_{kl}(Y))} \times \frac{\binom{m}{2} + \binom{n}{2}}{mn}. \quad (19)$$

The information about function values v and w for each transposition will be stored and updated sequentially. For each transposition, $2(m + n - 2)$ terms will be manipulated as opposed to total number of terms over a random permutation, $\binom{m+n}{2}$.

3 Application

3.1 Imaging data and pre-processing

The study included 23 children who suffered maltreatment in early life, and 31 age matched typically developing (non-maltreated) comparison children [14, 15, 39]. All subjects were scanned at the University of Wisconsin-Madison. The maltreated sample suffered early childhood neglect as they were initially raised in institutional setting; in such settings, there is a lack of toys or simulation, unresponsive caregiving, and an overall dearth of individualized care and attention [82]. These children were, however, then adopted and then move into normative caregiving environments. For the controls, we selected children without a history of maltreatment from families with similar ranges of socioeconomic statuses. The exclusion criteria include, among many others, congenital abnormalities (e.g., Down syndrome or cerebral palsy) and fetal alcohol syndrome (FAS). The average age for maltreated children was 11.26 ± 1.71 years while that of controls was 11.58 ± 1.61 years. This particular age range was selected since this development period is characterized by major regressive and progressive brain changes [39, 60]. There are 10 boys and 13 girls in the maltreated group and 18 boys and 13 girls in the control group. Groups did not statistically differ on age, pubertal stage, sex, or socio-economic status [39]. The average amount of time spent in institutional care by children was 2.5 years $\pm$ 1.4 years, with a range from 3 months to 5.4 years. Children were on average 3.2 years $\pm$ 1.9 months when they adopted, with a range of 3 months to 7.7 years.

T1-weighted MRI were collected using a 3T General Electric SIGNA scanner (Waukesha, WI) with a quadrature birdcage head coil. DTI were also collected in the same scanner using a cardiac-gated, diffusion-weighted, spin-echo, single-shot, EPI pulse sequence [39]. Diffusion tensor encoding was achieved using twelve optimum non-collinear encoding directions with a diffusion weighting of 1114 s/mm^2 and a non-DW T2-weighted reference image. Other imaging parameters were TE = 78.2 ms, 3 averages (NEX: magnitude averaging), and an image acquisition matrix of 120×120 over a field of view of 240×240 mm^2. The acquired voxel size of $2 \times 2 \times 3$ mm was interpolated to 0.9375 mm isotropic dimensions (256×256 in plane image matrix). To minimize field inhomogeneity and image artifacts, high order shimming and field map images were collected using a pair of non-EPI gradient echo images at two echo times: TE1 = 8 ms and TE2 = 11 ms.
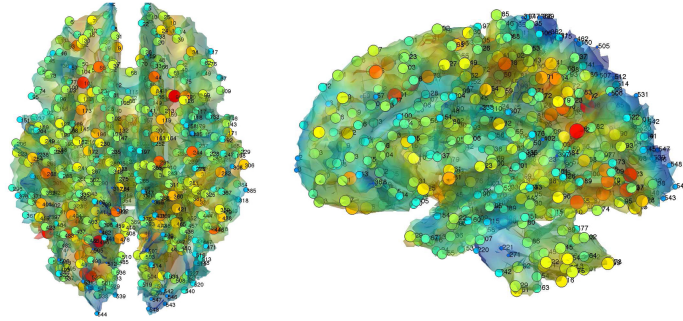
Jacobian determiants at 548 nodes
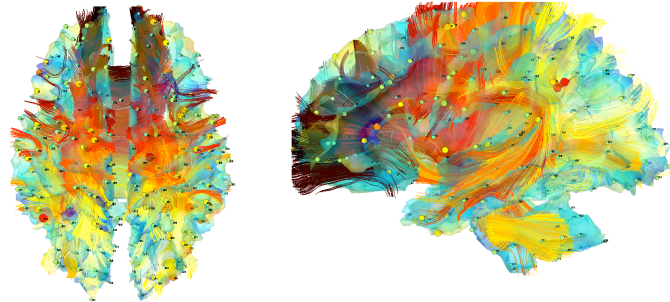
Fractional anisotropy at 548 nodes

Figure 4. 548 uniformly sampled nodes along the white matter surface. The nodes are sparsely sampled on the template white matter surface to guarantee there is no spurious high correlation due to proximity between nodes. The same nodes are taken in both MRI and DTI for comparison between the two modalities.

For MRI, a study specific template was constructed using the diffeomorphic shape and intensity averaging technique through Advanced Normalization Tools (ANTS) [3]. Image normalization of each individual image to the template was done using symmetric normalization with cross-correlation as the similarity metric. The 1mm resolution inverse deformation fields are then smoothed out with a Gaussian kernel of 4mm (full width at half maximum, FWHM). The Jacobian determinants of the inverse deformations from the template to individual subjects were computed at each voxel. The Jacobian determinants measure the amount of voxel-wise change from the template to the individual subjects [19]. White matter was also segmented into tissue probability maps using template-based priors, and registered to the template [5].

For diffuwion-MRI, images were corrected for eddy current related distortion and head motion via FSL software and distortions from field inhomogeneities were corrected using custom software based on the method given in [50] before performing a non-linear tensor estimation using CAMINO [7]. Subsequently, we have used iterative tensor image registration strategy for spatial normalization using DTI-ToolKit [51, 108]. Then fractional anisotropy (FA) were calculated for diffusion tensor volumes diffeomorphically registered to the study specific template.

We obtained the white matter tissue boundary sampled with 189536 mesh vertices and the average inter-nodal distance of 0.98mm. Since Jacobian determinant and FA values at neighboring voxels are highly correlated, 0.3% of the total mesh vertices are uniformly sampled to produce $p = 548$ nodes. This gives average inter-nodal distance of 15.7mm, which is large enough to avoid spurious high correlation between two adjacent nodes (Figure 4). We then computed 548×548 sample correlation matrices across

subjects.

3.2 Structural covariance network analysis

We sequentially thresholded correlation matrices and obtained graph filtrations. Figure 5 displays thresholded structural covariance networks at correlation 0.5 (A), 0.6 (B), 0.7 (C) and 0.8 (D). The structural covariance networks show very dense high correlation edges in maltreated children showing the highly homogenous nature of white matter structures for maltreated children. If FA and the Jacobian determinants are homogenous within a group, we should expect much higher correlation values.

Since there are only one correlation matrix per group, we applied the leave-one-out Jackknife resampling to generate multiple correlation matrices per group as follows. There are 31 normal controls and 23 maltreated children. For normal controls, we leave i-th subject out and compute the group level correlation matrix using the remaining 30 subjects. Let such correlation as w_i^{NC}. We repeat the process for all subjects and obtain correlation matrices $w_1^{NC}, \cdots, w_{31}^{NC}$ for the normal controls. For maltreated children, we also leave i-th subject out and compute the group level correlation using the remaining 22 subjects. Let such correlation be w_i^{Mal}. We repeat the process for all subjects and obtain correlation matrices $w_1^{Mal}, \cdots, w_{23}^{Mal}$ for the normal controls. The resampled correlation matrices are used in TDA and confirmatory fractal analysis later.

3.2.1 Topological structural covariance network analysis

Using the resampled correlation matrices of the Jacobian determinants and fractional anisotropy (FA) values on 548 nodes, we calculated the Betti-0 curves and Betti-1 curves for all subjects (Figure 5). The Betti-0 curves reveal higher values (more connected components) for the control group (than the maltreated group) at the same filtration values. This can only happen if brain regions are less correlated across regions in normal controls, an indication of more heterogeneous anatomical structure. On the other hand, Betti-1 curves for the maltreated group were higher than the control group (Figure 5). Hence, we have more loops for maltreated children compared to normal controls. This can only happen if there are more correlations and dense connections in structural covariate networks for maltreated children, again demonstrating more homogeneous nature of the structural covariate networks for maltreated children. Thus, using Betti-0 curves and Betti-1 curves, we are able to visualize the topological differences between maltreated and control participants by characterizing the connected components and loops. Therefore, the Betti curves can be used as a potential biomarker to distinguish between the maltreated subjects and control group.

To more rigorously quantify the topological differences, we used the Wasserstein distance based ratio statistic. First, we performed the Jackknife resampling. Then computed the between-group and within-group Wasserstein distances using D_W^{0D}, D_W^{1D} and $D_W^{0,1}$. Figure 6-right displays the distribution of between-group and within-group Wasserstein distances using D_W^{0D}. We notice a significant distinction between the Jackknife resampled Betti curves of both groups which is much larger than within-group variability using all three D_W^{0D}, D_W^{1D}, and $D_W^{0,1}$ distances and reveals the between group difference is highly significant. Figure 6-right clearly shows that the variability between groups is far larger than within-group variability. The p-values are very small (p-value < 0.001) for D_W^{0D}, D_W^{1D}, and $D_W^{0,1}$ for both Jacobian determinants and FA values. We conclude that there are significant topological differences in the topological structure of MRI and DTI structural covariance networks. Note our ratio test statistic is global test procedure over the range of filtration values and space so there in no need for multiple comparisons.
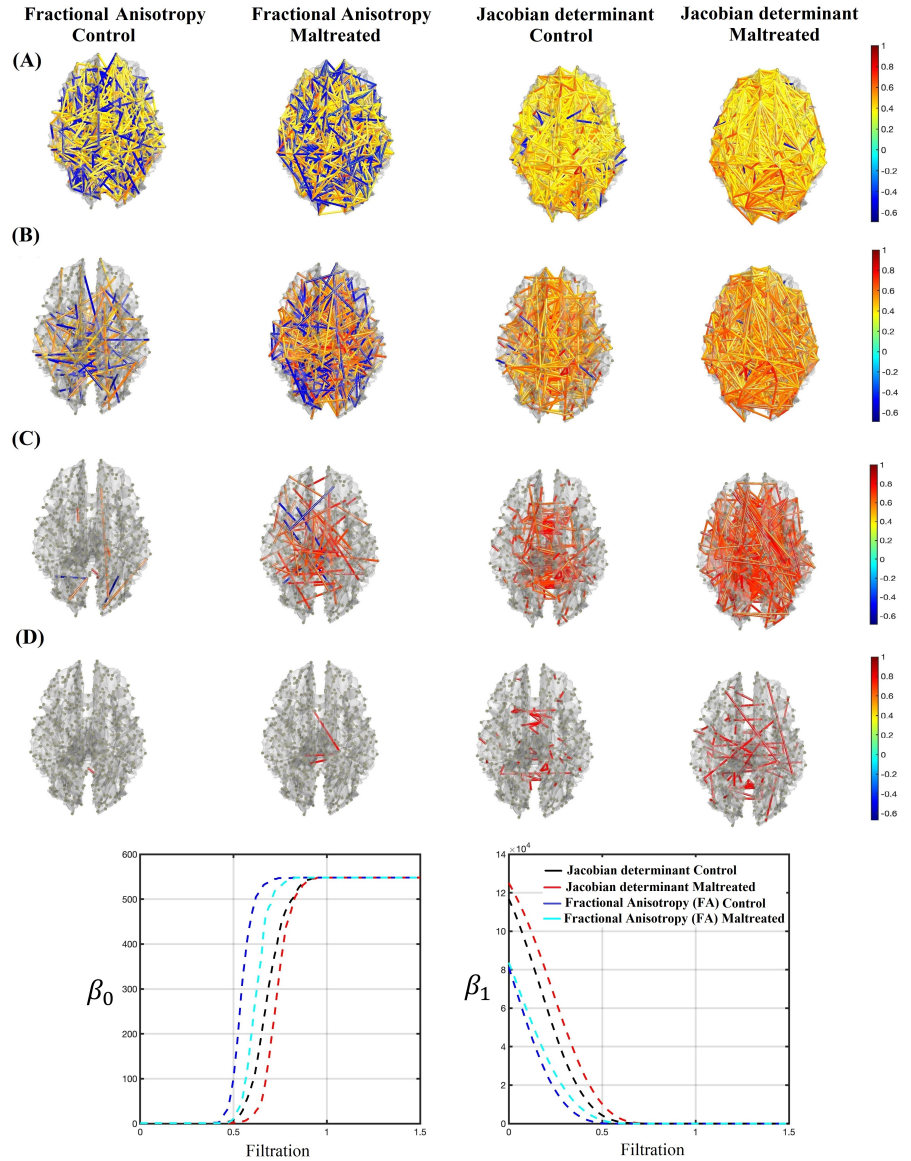
Figure 5. Top 4 Rows: 3D network visualization; These networks are obtained by thresholding structural covariance matrices for Jacobian determinant from MRI and fractional anisotropy (FA) from DTI at correlation 0.5 (A), 0.6 (B), 0.7 (B) and 0.8 (D). We have more dense connection patterns in maltreated subjects compared to control subjects. With increasing the sparsity parameter λ we have less dense network. Bottom Row: The averaged Betti curves of the brain network data for Jacobian determinant and Fractional Anisotropy (FA) on 548 node study. The Betti curves could recognize the difference between control group and maltreated group.

We also performed the rank-sum test on the areas under the continuous curves Betti-0 and Betti-1 to see whether we can differentiate between the two groups of normal control and maltreated group [14,15]. Rank-sum test checks the null hypothesis of no group difference, against the alternative that there is a group difference. According to our results, there exist statistically significant differences (p-value < 0.001) between the normal control and maltreated subjects. Therefore, using Betti curves we
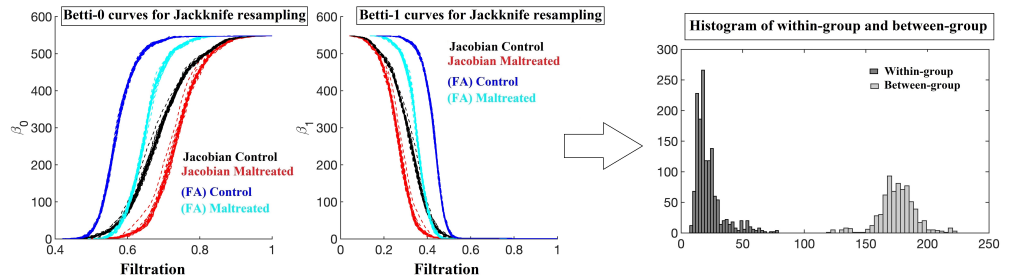
Figure 6. Top: The Betti curves of Jackknife resampled structural covariance networks. Bottom: The histogram of within- and between group 2-Wasserstein distance D_W^{0D} on Betti-0 and Betti-1 curves of resulting Jackknife resamples. The histogram clearly shows the huge variability across the groups relative to within groups.

could distinguish between TDA features in the structure covariance networks for maltreated children and the normal control.

4   Confirmatory fractal analysis

The human brain, as a complex multi-scale system, has been previously investigated in terms of its functional complexity using fractals. Fractal geometry is introduced by Benoit Mandelbrot in the 1980s [68]. Changes in the fractal geometry of biomedical data has been shown to have important implications in the diagnosis and prevention of disease [94]. Fractal analysis has been applied to study the spatiotemporal complexity of cerebral hemodynamics [44, 71]. Fractal analysis has been recognized as identifying a potential biomarker to measure the degree of brain damage in different neural diseases by estimating the neurological complexity of brain alterations [4, 23, 26, 35, 49, 106]. The complexity in the vascular structure of MRI scans in arteriovenous malformations (AVMs) disease has been assessed in terms of fractal characterization [28, 79]. Since fractal analysis has revealed less variations and smaller gender effect, it has been considered to be more robust than conventional volumetric methods in neurodegenerative disease detection [26, 106]. The brain signals of patients with Alzheimer's disease show less complexity compared to healthy controls [35, 49]. For patients with dementia, this reduced complexity is correlated with the degree of severity of disease [4]. Fractal information is also influential in the neural firing rates and vestibular responses of patients with Parkinson's disease (PD) and has produced significant results to differentiate patients with PD from normal controls [23].

Non-linearity at different scales and levels has been deemed to be one of the main properties of the human brain [21, 33, 93]. The permanent changes in geometric complexity of a maltreated child's brain function during early childhood may be quantified using the fractal geometry. There exists different methods to estimate the geometric complexity and fractal or complexity dimension of the brain imaging data. We show these methods significantly differentiate between different brain structural covariance networks.

Fractal geometry presents different measures to estimate the fractal dimension of an irregular set, for example, the well-known Minkowski dimension or box-counting dimension, among others [62]. Although box-counting methods have been used to successfully model many complex phenomena in nature, they often fail to determine the abrupt alterations which can occur in the structure of biomedical data [97]. Numerous efforts have been made to find more appropriate measure to detect these sudden changes, such as the Higuchi algorithm, power spectrum analysis, and Katz

algorithm [36, 46, 52]. Among all these fractal dimensional analysis approaches, we select the Higuchi algorithm for brain connectivity matrices. Higuchi's fractal dimension is a non-linear statistical measure which we can use to examine and discriminate the complexity of brain activity by relating complexity to different scales. In particular, we interpret larger fractal dimension estimates calculated using Higuchi's algorithm as corresponding to brain data structures with higher complexity. Higuchi's algorithm has been shown to be robust, reliable, and simple to implement [2]. In modeling and classifying the geometric complexity of neurological disease, fractal dimension estimation using the Higuchi algorithm provides reliable results [35, 77, 84]. This geometric complexity measure of data has been previously used to demonstrate the changes in dynamics of different brain pathologies [4, 23, 26, 35, 49, 106].

To measure the complexity of brain network data, we use the Higuchi method and apply it on the vectorized connectivity matrices of the brain network data. We extract the lower triangular portion of the original matrix which includes the main diagonal and all elements below (above) the diagonal. Next, we vectorize the extracted lower triangular matrix to convert the triangular matrix to column vectors. We then apply the Higuchi's algorithm as follows [46]. Let $w(1), w(2), \ldots, w(q)$ to be the the finite set of observations obtained from the vectorized lower (lower) triangular of the given connectivity matrix. From this set of observations, we construct a new vector of data, w_k^m, in the form:

$$w_k^m: \quad w(m), w(m+k), w(m+2k), \ldots, w(m + [\frac{q-m}{k}].k) \quad (m = 1, 2, \ldots, k) \quad (20)$$

where [ ] represents the Gauss' notation, q the number of columns or rows of the connectivity matrix (number of nodes), m and k are integers and k denotes the number of sets of new constructed data. We find the length of each set as follows:

$$L_m(k) = \frac{1}{k}(\sum_{i=1}^{[\frac{q-m}{k}]} |w(m+ik) - w(m+(i-1)k)|)(\frac{q-1}{[\frac{q-m}{k}]k}) \quad (21)$$

We estimate the fractal dimension by first computing the average length of the sets, $L(k) = average(L_m(k))$. Then, given data $L(k) \propto k^{-HFD}$, HFD is the Higuchi's fractal dimension and can be obtained by calculating the slope of the straight line that fits the values of $\log L(k)$ and $\log(k)$, i.e.,

$$HFD = \frac{\log L(k)}{\log(1/k)} \quad (22)$$

We calculated the Higuchi fractal dimension (HFD) for each network using the jackknife resampling technique. The HFD is 1.8940 ± 0.0006 for normal controls and 1.8719 ± 0.0031 for the maltreated children. We used the two-sample t-test in determining the statistical significance. The p-value for the two sided test is smaller than 0.001 indicating very strong group separation. The fractal analysis indicates a reduction in the complexity of the brain's function and geometry in the maltreated group compared to the control group, consistent with the topological network analysis result. The homogenous white mater structures in the maltreated children corresponds to reduced complexity.

Reduced geometric complexity has been previously reported for neurological diseases such as Alzheimer's disease and Parkinson's disease [35, 49]. This gives promise that such geometric complexity measures could be developed as potential biomarkers for clinical diagnosis. Further studies are needed, ideally using large population sizes, to report a clinical threshold in diagnosing maltreatment which could give rise to effectively finding a quantitative measure and clinical value as a biomarker for detecting

maltreatment. Our fractal analysis revealed statistically significant differences in the geometric complexity of structural covariate networks in maltreated children. The results suggest that brains affected by maltreatment in early childhood display lower complexity as measured by fractal dimension estimates in the white matter structures. This finding suggests that there is a strong correlation between brain structural abnormality and maltreatment in children.
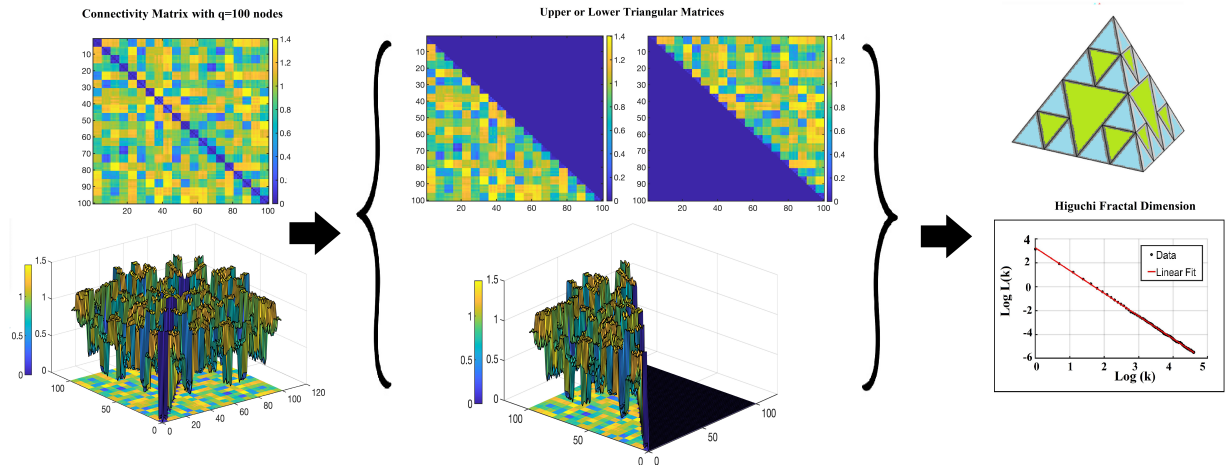

Figure 10. Application of Higuchi algorithm to estimate the geometric complexity of a given connectivity matrix of size 100×100. The lower triangular matrix is vectorized and feed into Higuchi algorithm.

Discussion

The human brain is a dynamic, complex and heterogeneous system which often calls for use of non-linear techniques for study and and analysis [21, 33, 93]. The human brain can be considered as a weighted graph or network, in which brain sites or regions of interest pare nodes of the network and connections between the sites or regions are edges of the network [92]. The topology, geometry and complex dynamics of the human brain can be comprehended using topological data analysis (TDA) and fractal analysis [27, 83]. Changes in topological structure and geometric complexity of brain networks could be a sign of possible brain disease or damage [26, 56, 65, 106].

Although TDA techniques such as persistent homology highlight the topological features in global structure [38, 83, 88] of different brain networks, they do not provide information about the geometric complexity [25, 27] of brain networks. Fractal geometry can be used to quantify the complexity in structural and functional patterns of the human brain [25, 27]. The fractal geometry framework presents a mathematical model to extract the variation in geometric complexity of different brain networks [26, 54, 55, 109]. Since child maltreatment may affect brain development during adolescence [11, 45], we model the changes in the local and global structure of brain networks at different scales using the both frameworks, TDA and fractal geometry.

Recent studies have suggested that early life stress, abuse and neglect can cause alteration in brain development [40, 48, 66, 74] and may increase the risk for poor mental health in adulthood. These deficits or potential harm to child's brain may influence the topological organizations of brain networks. To understand the topological features and global structure of brain network altered by maltreatment, we applied some frequently used methods in topological data analysis which helps to learn the impact of maltreatment on persistent homology features of the structural covariance networks. We

observed higher number of disconnected components for normal controls compared to maltreated children who experienced this stress in early childhood (Figure 5). The maltreated children's white matter structure had higher correlations associated with Jacobian determinants across white matter voxels than normal controls, which is indicative of higher anatomical homogeneity. Thus, when we threshold at a certain correlation value, more edges will be preserved for maltreated children; this leads to a smaller number of connected components. Maltreatment in early childhood is therefore, elated to denser structural covariance patterns at a specific threshold value. Our 3D network visualization in Figure 5 agreed with this conclusion.

In a study by [39], children who were suffering from neglect demonstrated disrupted white matter brain organization, which resulted in more diffused connections between brain regions. The less white matter directional organization seems to cause an increase in homogeneity of Jacobian determinants and fractional anisotropy (FA) across brain regions. Our proposed topology-based method was successful to reveal the alteration in topological pattern of brain white matter structures caused by abuse and neglect during child's brain development. We believe TDA could be effectively utilized as a biomarker to identify neurobiology related to maltreatment and maltreatment-related negative outcomes. We believe this study may lead to increase knowledge and insights toward the impact of maltreatment on brain development and most importantly child abuse and neglect prevention. The method can be applicable to neurological diseases such as AD and PD [4, 23, 35, 49].

In fractal analysis, we noticed a reduction in fractal or complexity dimension of maltreated child's brain white matter compared to control subjects, which indicates more homogeneous white matter structures in maltreated children. Our finding in using TDA and fractals are consistent. While there have been many different studies to quantify the geometric complexity of brain structure through fractals, [26, 54, 55, 109], it is unclear if fractal analysis can produce consistent results against TDA methods. This study offers some suggestions that they may produce similar results. The present study identifies two important altered brain characteristics in those that have suffered maltreatment, the topology and the geometric complexity, together, these characteristics provide essential information about the global and local structure of brain architecture. The altered topological structure of white matter was delineated using topological data analysis (TDA) methods, while the fractal geometry successfully detailed the varying geometric complexity of these same structures. This study could serve as a novel template and perspective for detecting altered topological structure, geometry and complexity in the brain's white matter. This study provides comprehensive models and frameworks to identify the impact of childhood maltreatment on brain structural covariance networks using rigorous mathematical techniques.

To develop a clinically accurate diagnostic tool, we need to extended our study to a larger population size, such as the Adolescent Brain Cognitive Development (ABCD) database, the largest long-term study of brain development and child health in US with more than 100 psychiatric and 11 cognitive measures. In the ABCD database, youth ($n =$11,875) 9-11 years of age were recruited for the study. This age range is important as it is a period of development critical to an individual's life trajectory. The incidence of psychiatric illnesses, such as attention deficit hyperactivity disorder (ADHD), anxiety, mood disorders, and psychosis, increases through adolescence [72]. The application of our methods to larger datasets such as the ABCD database is left as a future study.

Acknowledgements

of South Carolina for discussion on statistical methods. We also like to thank Vijay Anand of University of Exeter and Anass El Yaagoubi Bourakna for discussion on validation methods.

References

1. H. Adams, T. Emerson, M. Kirby, R. Neville, C. Peterson, P. Shipman, S. Chepushtanova, E. Hanson, F. Motta, and L. Ziegelmeier. Persistence images: A stable vector representation of persistent homology. *Journal of Machine Learning Research*, 18, 2017.

2. H. Ahammer, N. Sabathiel, and M. A. Reiss. Is a two-dimensional generalization of the higuchi algorithm really necessary? *Chaos: An Interdisciplinary Journal of Nonlinear Science*, 25(7):073104, 2015.

3. B. B. Avants, C. L. Epstein, M. Grossman, and J. C. Gee. Symmetric diffeomorphic image registration with cross-correlation: evaluating automated labeling of elderly and neurodegenerative brain. *Medical image analysis*, 12(1):26–41, 2008.

4. C. Besthorn, H. Sattel, C. Geiger-Kabisch, R. Zerfass, and H. Förstl. Parameters of eeg dimensional complexity in alzheimer's disease. *Electroencephalography and clinical neurophysiology*, 95(2):84–89, 1995.

5. M. F. Bonner and M. Grossman. Gray matter density of auditory association cortex relates to knowledge of sound concepts in primary progressive aphasia. *Journal of Neuroscience*, 32(23):7986–7991, 2012.

6. P. Bubenik and P. Dłotko. A persistence landscapes toolbox for topological statistics. *Journal of Symbolic Computation*, 78:91–114, 2017.

7. C. P. Camino. open-source diffusion-mri reconstruction and processing. In *14th Scientific Meeting of the International Society for Magnetic Resonance in Medicine. Seattle: International Society for Magnetic Resonance in Medicine*, 2006.

8. J. Cao and K. Worsley. The geometry of correlation fields with an application to functional connectivity of the brain. *The annals of applied probability*, 9(4):1021–1057, 1999.

9. L. Caputi, A. Pidnebesna, and J. Hlinka. Promises and pitfalls of topological data analysis for brain connectivity analysis. *NeuroImage*, 238:118245, 2021.

10. G. Carlsson and F. Mémoli. Persistent clustering and a theorem of j. kleinberg. *arXiv preprint arXiv:0808.2241*, 2008.

11. C. CB. Understanding the effects of maltreatment on brain development, 2015.

12. M. K. Chung. *Brain network analysis*. Cambridge University Press, 2019.

13. M. K. Chung, J. L. Hanson, N. Adluru, A. L. Alexander, R. J. Davidson, and S. D. Pollak. Integrative structural brain network analysis in diffusion tensor imaging. *Brain Connectivity*, 7(6):331–346, 2017.

14. M. K. Chung, J. L. Hanson, H. Lee, N. Adluru, A. L. Alexander, R. J. Davidson, and S. D. Pollak. Persistent homological sparse network approach to detecting white matter abnormality in maltreated children: Mri and dti multimodal study. In *Medical Image Computing and Computer-Assisted Intervention–MICCAI 2013: 16th International Conference, Nagoya, Japan, September 22-26, 2013, Proceedings, Part I 16*, pages 300–307. Springer, 2013.

15. M. K. Chung, J. L. Hanson, J. Ye, R. J. Davidson, and S. D. Pollak. Persistent homology in sparse regression and its application to brain morphometry. *IEEE transactions on medical imaging*, 34(9):1928–1939, 2015.

16. M. K. Chung, S.-G. Huang, A. Gritsenko, L. Shen, and H. Lee. Statistical inference on the number of cycles in brain networks. In *2019 IEEE 16th International Symposium on Biomedical Imaging (ISBI 2019)*, pages 113–116. IEEE, 2019.

17. M. K. Chung, H. Lee, A. DiChristofano, H. Ombao, and V. Solo. Exact topological inference of the resting-state brain networks in twins. *Network Neuroscience*, 3(3):674–694, 2019.

18. M. K. Chung, V. Singh, P. T. Kim, K. M. Dalton, and R. J. Davidson. Topological characterization of signal in brain images using min-max diagrams. In *International Conference on Medical Image Computing and Computer-Assisted Intervention*, pages 158–166. Springer, 2009.

19. M. K. Chung, K. J. Worsley, T. Paus, C. Cherif, D. L. Collins, J. N. Giedd, J. L. Rapoport, and A. C. Evans. A unified statistical approach to deformation-based morphometry. *NeuroImage*, 14(3):595–606, 2001.

20. M. K. Chung, L. Xie, S.-G. Huang, Y. Wang, J. Yan, and L. Shen. Rapid acceleration of the permutation test via transpositions. In *International workshop on connectomics in neuroimaging*, pages 42–53. Springer, 2019.

21. G. Claxton. *Intelligence in the flesh: Why your mind needs your body much more than it thinks*. Yale University Press, 2015.

22. M. Daianu, N. Jahanshad, T. M. Nir, C. R. Jack Jr, M. W. Weiner, M. A. Bernstein, P. M. Thompson, and A. D. N. Initiative. Rich club analysis in the alzheimer's disease connectome reveals a relatively undisturbed structural core network. *Human brain mapping*, 36(8):3087–3103, 2015.

23. Z. A. Dastgheib, B. Lithgow, and Z. Moussavi. Application of fractal dimension on vestibular response signals for diagnosis of parkinson's disease. In *2011 Annual International Conference of the IEEE Engineering in Medicine and Biology Society*, pages 7892–7895. IEEE, 2011.

24. C. Davatzikos, M. Vaillant, S. M. Resnick, J. L. Prince, S. Letovsky, and R. N. Bryan. A computerized approach for morphological analysis of the corpus callosum. *Journal of computer assisted tomography*, 20(1):88–97, 1996.

25. A. Di Ieva. Fractal analysis of microvascular networks in malignant brain tumors. *Clinical Neuropathology*, 31(5):342–351, 2012.

26. A. Di Ieva, F. J. Esteban, F. Grizzi, W. Klonowski, and M. Martín-Landrove. Fractals in the neurosciences, part ii: clinical applications and future perspectives. *The Neuroscientist*, 21(1):30–43, 2015.

27. A. Di Ieva et al. *The fractal geometry of the brain*, volume 22. Springer, 2016.

28. A. Di Ieva, E. M. Schmitz, and M. D. Cusimano. Analysis of intracranial pressure: past, present, and future. *The Neuroscientist*, 19(6):592–603, 2013.

29. A. Dubb, R. Gur, B. Avants, and J. Gee. Characterization of sexual dimorphism in the human corpus callosum. *Neuroimage*, 20(1):512–519, 2003.

30. H. Edelsbrunner, J. Harer, et al. Persistent homology-a survey. *Contemporary mathematics*, 453(26):257–282, 2008.

31. H. Edelsbrunner and J. L. Harer. *Computational topology: an introduction.* American Mathematical Society, 2022.

32. H. Edelsbrunner, D. Letscher, and A. Zomorodian. Topological persistence and simplification. In *Proceedings 41st annual symposium on foundations of computer science*, pages 454–463. IEEE, 2000.

33. M. D. Fox, A. Z. Snyder, J. L. Vincent, M. Corbetta, D. C. Van Essen, and M. E. Raichle. The human brain is intrinsically organized into dynamic, anticorrelated functional networks. *Proceedings of the National Academy of Sciences*, 102(27):9673–9678, 2005.

34. R. Ghrist. Barcodes: the persistent topology of data. *Bulletin of the American Mathematical Society*, 45(1):61–75, 2008.

35. C. Gómez, Á. Mediavilla, R. Hornero, D. Abásolo, and A. Fernández. Use of the higuchi's fractal dimension for the analysis of meg recordings from alzheimer's disease patients. *Medical engineering & physics*, 31(3):306–313, 2009.

36. R. S. Gomolka, S. Kampusch, E. Kaniusas, F. Thürk, J. C. Széles, and W. Klonowski. Higuchi fractal dimension of heart rate variability during percutaneous auricular vagus nerve stimulation in healthy and diabetic subjects. *Frontiers in physiology*, 9:1162, 2018.

37. Z. Gracia-Tabuenca, J. C. Díaz-Patiño, I. Arelio, and S. Alcauter. Topological data analysis reveals robust alterations in the whole-brain and frontal lobe functional connectomes in attention-deficit/hyperactivity disorder. *eneuro*, 7(3), 2020.

38. M. Gromov. *Local and global in geometry.* Institut des Hautes Etudes Scientifiques [IHES], 1999.

39. J. L. Hanson, N. Adluru, M. K. Chung, A. L. Alexander, R. J. Davidson, and S. D. Pollak. Early neglect is associated with alterations in white matter integrity and cognitive functioning. *Child development*, 84(5):1566–1578, 2013.

40. J. L. Hanson, M. K. Chung, B. B. Avants, K. D. Rudolph, E. A. Shirtcliff, J. C. Gee, R. J. Davidson, and S. D. Pollak. Structural variations in prefrontal cortex mediate the relationship between early childhood stress and spatial working memory. *Journal of Neuroscience*, 32(23):7917–7925, 2012.

41. J. L. Hanson, M. K. Chung, B. B. Avants, E. A. Shirtcliff, J. C. Gee, R. J. Davidson, and S. D. Pollak. Early stress is associated with alterations in the orbitofrontal cortex: a tensor-based morphometry investigation of brain structure and behavioral risk. *Journal of neuroscience*, 30(22):7466–7472, 2010.

42. Y. He, Z. Chen, and A. Evans. Structural insights into aberrant topological patterns of large-scale cortical networks in alzheimer's disease. *Journal of Neuroscience*, 28(18):4756–4766, 2008.

43. Y. He, Z. J. Chen, and A. C. Evans. Small-world anatomical networks in the human brain revealed by cortical thickness from mri. *Cerebral cortex*, 17(10):2407–2419, 2007.

44. P. Hermán, L. Kocsis, and A. Eke. Fractal branching pattern in the pial vasculature in the cat. *Journal of Cerebral Blood Flow & Metabolism*, 21(6):741–753, 2001.

45. R. J. Herringa, R. M. Birn, P. L. Ruttle, C. A. Burghy, D. E. Stodola, R. J. Davidson, and M. J. Essex. Childhood maltreatment is associated with altered fear circuitry and increased internalizing symptoms by late adolescence. *Proceedings of the National Academy of Sciences*, 110(47):19119–19124, 2013.

46. T. Higuchi. Approach to an irregular time series on the basis of the fractal theory. *Physica D: Nonlinear Phenomena*, 31(2):277–283, 1988.

47. C. E. Hostinar, S. A. Stellern, C. Schaefer, S. M. Carlson, and M. R. Gunnar. Associations between early life adversity and executive function in children adopted internationally from orphanages. *Proceedings of the National Academy of Sciences*, 109(supplement_2):17208–17212, 2012.

48. A. P. Jackowski, C. M. De Araújo, A. L. T. De Lacerda, J. de Jesus Mari, and J. Kaufman. Neurostructural imaging findings in children with post-traumatic stress disorder: Brief review. *Psychiatry and clinical neurosciences*, 63(1):1–8, 2009.

49. J. Jeong. Eeg dynamics in patients with alzheimer's disease. *Clinical neurophysiology*, 115(7):1490–1505, 2004.

50. P. Jezzard and S. Clare. Sources of distortion in functional mri data. *Human brain mapping*, 8(2-3):80–85, 1999.

51. S. Joshi, B. Davis, M. Jomier, and G. Gerig. Unbiased diffeomorphic atlas construction for computational anatomy. *NeuroImage*, 23:S151–S160, 2004.

52. M. J. Katz. Fractals and the analysis of waveforms. *Computers in biology and medicine*, 18(3):145–156, 1988.

53. A. Khalid, B. S. Kim, M. K. Chung, J. C. Ye, and D. Jeon. Tracing the evolution of multi-scale functional networks in a mouse model of depression using persistent brain network homology. *NeuroImage*, 101:351–363, 2014.

54. C. C. King. Fractal and chaotic dynamics in nervous systems. *Progress in neurobiology*, 36(4):279–308, 1991.

55. V. G. Kiselev, K. R. Hahn, and D. P. Auer. Is the brain cortex a fractal? *Neuroimage*, 20(3):1765–1774, 2003.

56. L. Kuang, Y. Gao, Z. Chen, J. Xing, F. Xiong, and X. Han. White matter brain network research in alzheimer's disease using persistent features. *Molecules*, 25(11):2472, 2020.

57. D. S. Lee. Clinical personal connectomics using hybrid pet/mri. *Nuclear Medicine and Molecular Imaging*, 53(3):153–163, 2019.

58. H. Lee, M. K. Chung, H. Kang, B.-N. Kim, and D. S. Lee. Computing the shape of brain networks using graph filtration and gromov-hausdorff metric. In *Medical Image Computing and Computer-Assisted Intervention–MICCAI 2011: 14th International Conference, Toronto, Canada, September 18-22, 2011, Proceedings, Part II 14*, pages 302–309. Springer, 2011.

59. H. Lee, H. Kang, M. K. Chung, B.-N. Kim, and D. S. Lee. Persistent brain network homology from the perspective of dendrogram. *IEEE transactions on medical imaging*, 31(12):2267–2277, 2012.

60. R. K. Lenroot and J. N. Giedd. Brain development in children and adolescents: insights from anatomical magnetic resonance imaging. *Neuroscience & biobehavioral reviews*, 30(6):718–729, 2006.

61. J. P. Lerch, K. Worsley, W. P. Shaw, D. K. Greenstein, R. K. Lenroot, J. Giedd, and A. C. Evans. Mapping anatomical correlations across cerebral cortex (macacc) using cortical thickness from mri. *Neuroimage*, 31(3):993–1003, 2006.

62. J. Li, Q. Du, and C. Sun. An improved box-counting method for image fractal dimension estimation. *Pattern recognition*, 42(11):2460–2469, 2009.

63. C. Liu, X. Ma, J. Wang, J. Zhang, H. Zhang, S. Xie, and D. Yu. Neurophysiological assessment of image quality from eeg using persistent homology of brain network. In *2021 IEEE International Conference on Multimedia and Expo (ICME)*, pages 1–6. IEEE, 2021.

64. Y. Liu, Y. Duan, Y. He, J. Wang, M. Xia, C. Yu, H. Dong, J. Ye, H. Butzkueven, K. Li, et al. Altered topological organization of white matter structural networks in patients with neuromyelitis optica. *PloS one*, 7(11):e48846, 2012.

65. C.-Y. Lo, P.-N. Wang, K.-H. Chou, J. Wang, Y. He, and C.-P. Lin. Diffusion tensor tractography reveals abnormal topological organization in structural cortical networks in alzheimer's disease. *Journal of Neuroscience*, 30(50):16876–16885, 2010.

66. M. M. Loman, A. E. Johnson, A. Westerlund, S. D. Pollak, C. A. Nelson, and M. R. Gunnar. The effect of early deprivation on executive attention in middle childhood. *Journal of Child Psychology and Psychiatry*, 54(1):37–45, 2013.

67. A. M. C. Machado and J. C. Gee. Atlas warping for brain morphometry. In *Medical Imaging 1998: Image Processing*, volume 3338, pages 642–651. SPIE, 1998.

68. B. B. Mandelbrot and B. B. Mandelbrot. *The fractal geometry of nature*, volume 1. WH freeman New York, 1982.

69. E. McCrory, S. A. De Brito, and E. Viding. Research review: the neurobiology and genetics of maltreatment and adversity. *Journal of child psychology and psychiatry*, 51(10):1079–1095, 2010.

70. NSCDC. Early experiences can alter gene expression and affect long-term development (working paper 10). 2010a.

71. R. B. Panerai. Complexity of the human cerebral circulation. *Philosophical Transactions of the Royal Society A: Mathematical, Physical and Engineering Sciences*, 367(1892):1319–1336, 2009.

72. T. Paus, M. Keshavan, and J. N. Giedd. Why do many psychiatric disorders emerge during adolescence? *Nature reviews neuroscience*, 9(12):947–957, 2008.

73. M. Piangerelli, M. Rucco, L. Tesei, and E. Merelli. Topological classifier for detecting the emergence of epileptic seizures. *BMC research notes*, 11(1):1–7, 2018.

74. S. D. Pollak. Mechanisms linking early experience and the emergence of emotions: Illustrations from the study of maltreated children. *Current directions in psychological science*, 17(6):370–375, 2008.

75. A. Qiu, A. Lee, M. Tan, and M. K. Chung. Manifold learning on brain functional networks in aging. *Medical image analysis*, 20(1):52–60, 2015.

76. T. Qiu, X. Luo, Z. Shen, P. Huang, X. Xu, J. Zhou, M. Zhang, A. D. N. Initiative, et al. Disrupted brain network in progressive mild cognitive impairment measured by eigenvector centrality mapping is linked to cognition and cerebrospinal fluid biomarkers. *Journal of Alzheimer's Disease*, 54(4):1483–1493, 2016.

77. M. Radhakrishnan, D. Won, T. A. Manoharan, V. Venkatachalam, R. M. Chavan, and H. D. Nalla. Investigating electroencephalography signals of autism spectrum disorder (asd) using higuchi fractal dimension. *Biomedical Engineering/Biomedizinische Technik*, 66(1):59–70, 2021.

78. A. Rao, P. Aljabar, and D. Rueckert. Hierarchical statistical shape analysis and prediction of sub-cortical brain structures. *Medical image analysis*, 12(1):55–68, 2008.

79. G. Reishofer, K. Koschutnig, C. Enzinger, F. Ebner, and H. Ahammer. Fractal dimension and vessel complexity in patients with cerebral arteriovenous malformations. *PLoS One*, 7(7):e41148, 2012.

80. M. Rubinov and O. Sporns. Complex network measures of brain connectivity: uses and interpretations. *Neuroimage*, 52(3):1059–1069, 2010.

81. M. Rucco, F. Castiglione, E. Merelli, and M. Pettini. Characterisation of the idiotypic immune network through persistent entropy. In *Proceedings of ECCS 2014*, pages 117–128. Springer, 2016.

82. M. Rutter et al. Developmental catch-up, and deficit, following adoption after severe global early privation. *The Journal of Child Psychology and Psychiatry and Allied Disciplines*, 39(4):465–476, 1998.

83. F. A. Santos, E. P. Raposo, M. D. Coutinho-Filho, M. Copelli, C. J. Stam, and L. Douw. Topological phase transitions in functional brain networks. *Physical Review E*, 100(3):032414, 2019.

84. E. Shamsi, M. A. Ahmadi-Pajouh, and T. S. Ala. Higuchi fractal dimension: An efficient approach to detection of brain entrainment to theta binaural beats. *Biomedical Signal Processing and Control*, 68:102580, 2021.

85. J. P. Shonkoff, A. S. Garner, C. on Psychosocial Aspects of Child, A. Family Health, Committee on Early Childhood, D. Care, S. on Developmental, B. Pediatrics, B. S. Siegel, M. I. Dobbins, M. F. Earls, A. S. Garner, L. McGuinn, J. Pascoe, and D. L. Wood. The lifelong effects of early childhood adversity and toxic stress. *Pediatrics*, 129(1):e232–e246, 2012.

86. N. Shu, Y. Liu, J. Li, Y. Li, C. Yu, and T. Jiang. Altered anatomical network in early blindness revealed by diffusion tensor tractography. *PloS one*, 4(9):e7228, 2009.

87. G. Singh, F. Memoli, T. Ishkhanov, G. Sapiro, G. Carlsson, and D. L. Ringach. Topological analysis of population activity in visual cortex. *Journal of vision*, 8(8):11–11, 2008.

88. A. E. Sizemore, J. E. Phillips-Cremins, R. Ghrist, and D. S. Bassett. The importance of the whole: topological data analysis for the network neuroscientist. *Network Neuroscience*, 3(3):656–673, 2019.

89. V. Solo, J.-B. Poline, M. A. Lindquist, S. L. Simpson, F. D. Bowman, M. K. Chung, and B. Cassidy. Connectivity in fmri: blind spots and breakthroughs. *IEEE transactions on medical imaging*, 37(7):1537–1550, 2018.

90. T. Songdechakraiwut, B. M. Krause, M. I. Banks, K. V. Nourski, and B. D. Van Veen. Topological classification in a wasserstein distance based vector space. *arXiv preprint arXiv:2202.01275*, 2022.

91. T. Songdechakraiwut, L. Shen, and M. Chung. Topological learning and its application to multimodal brain network integration. In *Medical Image Computing and Computer Assisted Intervention–MICCAI 2021: 24th International Conference, Strasbourg, France, September 27–October 1, 2021, Proceedings, Part II 24*, pages 166–176. Springer, 2021.

92. O. Sporns. Network analysis, complexity, and brain function. *Complexity*, 8(1):56–60, 2002.

93. M. Taubert, B. Draganski, A. Anwander, K. Müller, A. Horstmann, A. Villringer, and P. Ragert. Dynamic properties of human brain structure: learning-related changes in cortical areas and associated fiber connections. *Journal of Neuroscience*, 30(35):11670–11677, 2010.

94. C. Thamrin, G. Stern, and U. Frey. Fractals for physicians. *Paediatric respiratory reviews*, 11(2):123–131, 2010.

95. P. Thompson, J. N. Giedd, R. E. Blanton, C. Lindshield, S. Badrtalei, R. P. Woods, D. MacDonald, A. C. Evans, and A. W. Toga. Growth patterns in the developing human brain detected using continuum-mechanical tensor maps and serial mri. *NeuroImage*, 7(4):S38, 1998.

96. P. Thompson and A. W. Toga. Anatomically driven strategies for high-dimensional brain image warping and pathology detection. *Brain warping*, pages 311–336, 1998.

97. R. G. Turcott and M. C. Teich. Fractal character of the electrocardiogram: distinguishing heart-failure and normal patients. *Annals of biomedical engineering*, 24(2):269–293, 1996.

98. USDHHS. Persistent fear and anxiety can affect young children's learning and development: Working paper no. 9. *US Department of Health and Human Services*, 2010.

99. B. C. Van Wijk, C. J. Stam, and A. Daffertshofer. Comparing brain networks of different size and connectivity density using graph theory. *PloS one*, 5(10):e13701, 2010.

100. Y. Wang, H. Ombao, and M. K. Chung. Statistical persistent homology of brain signals. In *ICASSP 2019-2019 IEEE International Conference on Acoustics, Speech and Signal Processing (ICASSP)*, pages 1125–1129. IEEE, 2019.

101. L. Wasserman. Topological data analysis. *Annual Review of Statistics and Its Application*, 5:501–532, 2018.

102. WHO. Child maltreatment. *World Health Organization (WHO)*, 2022.

103. K. R. Wilson, D. J. Hansen, and M. Li. The traumatic stress response in child maltreatment and resultant neuropsychological effects. *Aggression and Violent Behavior*, 16(2):87–97, 2011.

104. K. J. Worsley, A. Charil, J. Lerch, and A. C. Evans. Connectivity of anatomical and functional mri data. In *Proceedings. 2005 IEEE International Joint Conference on Neural Networks, 2005.*, volume 3, pages 1534–1541. IEEE, 2005.

105. K. J. Worsley, J.-I. Chen, J. Lerch, and A. C. Evans. Comparing functional connectivity via thresholding correlations and singular value decomposition. *Philosophical Transactions of the Royal Society B: Biological Sciences*, 360(1457):913–920, 2005.

106. Y.-T. Wu, K.-K. Shyu, C.-W. Jao, Z.-Y. Wang, B.-W. Soong, H.-M. Wu, and P.-S. Wang. Fractal dimension analysis for quantifying cerebellar morphological change of multiple system atrophy of the cerebellar type (msa-c). *Neuroimage*, 49(1):539–551, 2010.

107. J. Xing, J. Jia, X. Wu, and L. Kuang. A spatiotemporal brain network analysis of alzheimer's disease based on persistent homology. *Frontiers in Aging Neuroscience*, 14, 2022.

108. H. Zhang, B. B. Avants, P. A. Yushkevich, J. H. Woo, S. Wang, L. F. McCluskey, L. B. Elman, E. R. Melhem, and J. C. Gee. High-dimensional spatial normalization of diffusion tensor images improves the detection of white matter differences: an example study using amyotrophic lateral sclerosis. *IEEE transactions on medical imaging*, 26(11):1585–1597, 2007.

109. L. Zhang, J. Z. Liu, D. Dean, V. Sahgal, and G. H. Yue. A three-dimensional fractal analysis method for quantifying white matter structure in human brain. *Journal of neuroscience methods*, 150(2):242–253, 2006.

110. X. Zhu, H.-I. Suk, and D. Shen. Matrix-similarity based loss function and feature selection for alzheimer's disease diagnosis. In *Proceedings of the IEEE Conference on Computer Vision and Pattern Recognition*, pages 3089–3096, 2014.

111. A. J. Zomorodian. *Topology for computing*, volume 16. Cambridge university press, 2005.